of the curving flow of the Minnesota Glacier (Fig. 1). Where the flow traces are aligned along the *y* direction, the flow is perpendicular to the radar beam and the line-of-sight velocity component is zero. This criterion, applied to the flow traces and fringes near (69, 21), selects a zero-velocity fringe that differs by about 2 fringes from the one chosen at (26, 3).
21. In relation to the data averaging and condensing procedure described in (*13*), a smaller pixel size (16 m by 20 m) was obtained by averaging only in groups of four original pixels in the cross-range direction and doing no averaging in the range direction.
22. This is probably because interference cannot be obtained when the local rotation or rotational shear exceeds a certain limit. The shear is near the limit in Fig. 2 and exceeds it where the marginal zones are narrower. A similar limit was encountered in an SRI image of the Landers earthquake area (*9*): The fringes disappeared in a zone near the fault, where the shear strain was greatest. The rotation limit is when the *x* or *y* gradient of the line-of-sight displacement field is so large that each pixel contains a range of line-of-sight displacements spanning half a wavelength. The limit can be reduced with a reduction of the pixel size, as in Fig. 2. With a shorter time interval between SAR images (3 days in the case of ERS-1), the amount of rotation attributable to the shear flow of ice can be reduced in an effort to get below the limit.
23. A. M. Smith, *J. Glaciol.* **37**, 51 (1991).
24. This calculation was kindly done by C. S. M. Doake (personal communication).
25. Choice of the grounding line at coordinate 128 km is appropriate because $d\Delta z/dx = 0$ there on the observed curve (Fig. 3), which is what the model (*23*) assumes at $x = 0$. Because the model has $\Delta z = 0$ there, the uplift values on the calculated (dotted) curve are obtained by adding $\Delta z(x)$ from Eq. 1 to the observed uplift value (-0.05 m) at 128 km.
26. Very close agreement is not expected because the model assumes a two-dimensional flexure geometry, whereas the actual geometry is decidedly three-dimensional, with a tongue of grounded ice surrounded on three sides by floating ice that participates in tidal flexure (Fig. 1B).
27. The indication of grounding-line retreat in Fig. 4 is dependent on how the solid and dashed curves are positioned in relation to the indicated latitude and longitude lines. For the solid curve, the interferogram (Fig. 1A) was rescaled to the scale of the satellite image map (*18*) on the basis of image parameters furnished by ESA, and a transparency of the interferogram was registered to the map by registering the ice stream margins and the Flowers Hills. The latitude and longitude lines from the map were then transferred to the interferogram, on which the grounding line was drawn on the basis of the fringe pattern. For the dashed curve, the longitude and latitude lines in fig. 2 of (*17*) were transferred to fig. 5 of (*17*) with, as a reference, the frame of fig. 5 that is shown in fig. 2; after rescaling, we could position the grounding line in fig. 5 of (*17*) in our Fig. 4 by registering the latitude and longitude lines. Besides the uncertainties involved in the above procedure, the comparison in our Fig. 4 is made further uncertain by problematical aspects of the ground-based determination of the grounding line, as indicated by comparison of the results of (*17*) and (*24*).
28. H. J. Zwally *et al.*, *Science* **246**, 1587 (1989); C. J. van der Veen, *Rev. Geophys.* **29**, 433 (1991); D. J. Wingham *et al.*, *Eos* **74**, 113 (1993).
29. Although displacement resolution in SRI (conservatively ~1 cm for horizontal displacements) is much finer than in SSI (~30 m or 4.5 m) (*31*), for the measurement of ice flow velocities this advantage is offset by a limitation on the time interval between the SAR images usable by SRI, which is the time over which a velocity is measured. A 6-day interval has given SRI interference, but 12-day or longer intervals have not. In SSI, by contrast, optical images taken 2 years apart were usable in velocity determination (*3*). The reason for the limitation on SRI is that ongoing or occasional changes in the scattering surface caused by snow ablation or accumulation at the radar wavelength scale become extensive enough in about a week's time to destroy the detailed phase coherence between the two images on which the interference depends (*32*). In SSI, on the other hand, the changes have to be substantial on the pixel scale (~30 m) before velocity measurement is prevented. This tends to occur first in the marginal shear zones (*3*). The result of the above tradeoffs is a velocity resolution of about 0.6 m year^{-1} for SRI and about 2.3 m year^{-1} for SSI (*3*). For a shorter time interval between images, the velocity resolution will be correspondingly poorer.
30. An important element of glacier flow mechanics to which SRI and SSI data can readily make a contribution, because it requires only relative rather than absolute velocities, is analysis of the strain-rate field of the ice; C. J. van der Veen and I. M. Whillans, *J. Glaciol.* **35**, 53 (1989); *ibid.* **36**, 324 (1990).
31. The figure ~30 m represents pixel-scale resolution. Bindschadler and Scambos (*3*) achieved subpixel resolution (±4.5 m) by a cross-correlation method, and Crippen (*11*) cites examples of 0.05-pixel precision in sequential imaging applied to tectonic deformation.
32. In the recent report of SRI applied to ground displacement in the Landers earthquake (*9*), there is an interferogram from two images taken 105 days apart, which suggests that coherence-destroying changes of the ground surface in that area accumulate much more slowly than they do in the area of the Rutford Ice Stream.
33. The additional limitation of SRI to detection of motion only in the line-of-sight direction of the radar beam means that only one component of the horizontal flow can be directly measured from an image pair, whereas SSI obtains the full horizontal velocity. The limitation on SRI can be circumvented wherever the direction of the velocity vector is established by flow traces, as in Minnesota Glacier and the adjacent ice stream, or wherever the vector can reasonably be assumed parallel to a nearby ice stream margin. The limitation could also be overcome by a second interferogram with a roughly perpendicular line of sight, but this may or may not be obtainable, depending on the orbital and operational features of the satellite. However, because the ice stream motions and the motion sensitivity of SRI are so large, the measurement of one velocity component within, say, 60° of the flow direction would be sufficient for the monitoring of ice stream flow changes.
34. The repeatability is given as ~0.25 m by R. A. Bindschadler, H. J. Zwally, J. A. Major, and A. C. Brenner [*NASA Spec. Publ. SP-503* (National Aeronautics and Space Administration, Washington, DC, 1989)].
35. D. D. Blankenship, R. E. Bell, V. A. Childers, S. M. Hodge, *Eos* **73**, 129 (1992).
36. R. A. Massom, *Satellite Remote Sensing of Polar Regions* (Belhaven, London, 1991); see also R. M. Thomas, "Satellite Remote Sensing for Ice Sheet Research," *NASA Tech. Memo. 86233* (National Aeronautics and Space Administration, Washington, DC, 1985).
37. National Research Council Ad Hoc Committee on the Relation between Land Ice and Sea Level, *Glaciers, Ice Sheets, and Sea Level: Effect of a CO_2-Induced Climatic Change* (National Academy Press, Washington, DC, 1985); R. A. Warrick and J. Oerlemans, in *Climate Change: The IPCC Scientific Assessment*, J. T. Houghton, G. J. Jenkins, J. J. Ephraums, Eds. (Cambridge Univ. Press, Cambridge, 1990); R. A. Bindschadler, Ed., "West Antarctic Ice Sheet Initiative," *NASA Conf. Publ. 3115* (National Aeronautics and Space Administration, Washington, DC, 1991).
38. Research carried out in part by the Jet Propulsion Laboratory, California Institute of Technology, under a contract with the National Aeronautics and Space Administration. We thank ESA for making the SAR images available.

Greenland Ice Sheet Surface Properties and Ice Dynamics from ERS-1 SAR Imagery

Mark Fahnestock, Robert Bindschadler, Ron Kwok, Ken Jezek

C-band synthetic aperture radar (SAR) imagery from the European Space Agency's ERS-1 satellite reveals the basic zonation of the surface of the Greenland Ice Sheet. The zones have backscatter signatures related to the structure of the snowpack, which varies with the balance of accumulation and melt at various elevations. The boundaries of zones can be accurately located with the use of this high-resolution imagery. The images also reveal a large flow feature in northeast Greenland that is similar to ice streams in Antarctica and may play a major role in the discharge of ice from the ice sheet.

Understanding the current state of balance of ice sheets requires monitoring their mass exchange processes. An ice sheet's mass balance (*1*) primarily depends on snowfall, loss of mass due to surface melting and subsequent runoff, and the calving of icebergs from outlet glaciers which reach the sea. Measurement of the mass balance of an ice sheet is not simple. Changes in the margins of the ice sheet reflect a complex integration of fluctuating input, internal flow, and discharge processes that operate at different characteristic time scales. While it is not easy to measure directly a small change in the geometry of an entire ice sheet, it is

M. Fahnestock and R. Bindschadler are at the National Aeronautics and Space Administration Goddard Space Flight Center (NASA/GSFC), Greenbelt, MD 20771. R. Kwok is with the Jet Propulsion Laboratory, California Institute of Technology, Pasadena, CA 91109. K. Jezek is with the Byrd Polar Research Center, Ohio State University, Columbus, OH 43210.

possible to look for changes in input processes and attempt to relate these changes to changing climatic conditions that will have an effect on the mass balance in the long term.

Recent changes in input conditions would show up most quickly as changes in the patterns of surface melt and accumulation. Synthetic aperture radar (SAR) imagery provides a view of the effects of these processes on the snowpack over an entire ice sheet. While these data are not directly related to mass accumulation or ablation, variations in these patterns can provide an indication of changing input conditions on a near-continental scale.

Surface melting is extensive on the Greenland Ice Sheet. Spatial variation in the effects of this melting enabled Benson (*2*) to divide the snow pack of the Greenland Ice Sheet into distinct diagenetic facies, or zones, on the basis of properties observed in snow pits and cores. These facies, which are described below, result from differential diagenesis of the snowpack caused by variations in the amounts of surface melt and accumulation, both of which vary with elevation, latitude, and local climate. Benson extrapolated the location of the zones around Greenland on the basis of point observations, poorly known surface elevation, and a representative atmospheric lapse rate.

Several of the boundaries between the zones are distinct and, as Benson suggested, changes in their locations should provide a sensitive indicator of change in local climatic conditions. Because of the low surface slope of the ice sheet, typically 0.01, changes in temperature that cause shifts in the elevation of these boundaries will also result in large lateral shifts of boundary positions, which should be easily observable in satellite imagery (*3*). Monitoring the locations of the boundaries between these zones can reveal changes in the input conditions long before they result in a change in ice-sheet geometry or dynamics.

Snow Facies in SAR Imagery

Zones are clearly apparent in early and late winter SAR scenes (Fig. 1) (*4*). The large-scale structure of the zones, reflected in variations in radar backscatter (image brightness), correspond closely to elevation, which is to be expected as the zones are related to the amount of surface melting. Backscatter strength can vary with the dielectric properties of the material, as a result of wetness or changes in conductivity, and also with variations in geometric properties such as roughness, grain size, and internal structure. The large-scale variations in backscatter over the ice sheet show a pattern that is similar to Benson's determination of facies; this similarity suggests that the set of physical parameters he observed are in some way responsible for the regional brightness patterns in the imagery.

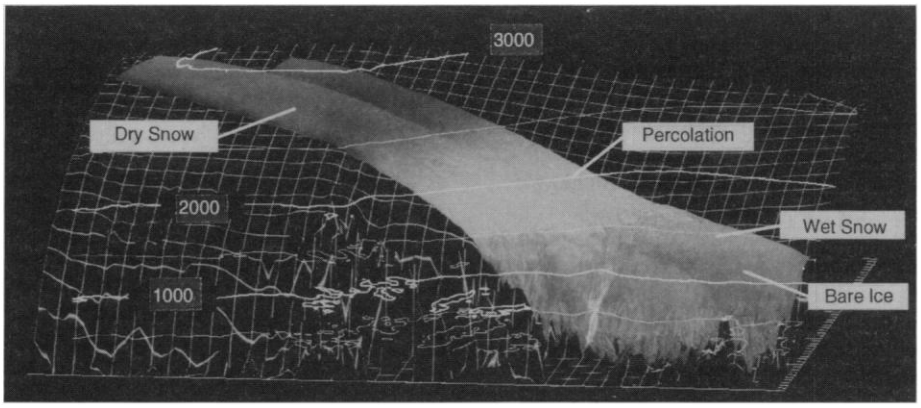

Fig. 1. A mosaic of 18 ERS-1 SAR scenes from two separate orbits, draped over a digital elevation model of the western Greenland Ice Sheet. The four regions of distinct radar backscatter have been labeled with Benson's correlative snow facies. Vertical exaggeration is 100:1, contour interval 500 m, grid spacing 25 km. The view is looking eastward toward the west coast between 67° and 74° N latitude.

The dry snow zone of the high interior produces little backscatter of the transmitted signal and thus appears dark. The cold snow pack, which is unmodified by meltwater, has a low density and relatively uniform small grain size. The fine grain size causes little volume scattering of the C-band signal (5.3 GHz; 5.7-cm wavelength) used by the ERS-1 SAR.

Below the dry snow zone (at lower elevations) is a region with the brightest regional returns from the ice sheet. This region is the percolation zone, where surface meltwater percolates downward, occasionally spreading out into layers. Freezing of this water in the surrounding cold firn transforms this drainage network into a set of vertical fingers or pipes and horizontal ice lenses. Surface scattering of the radar signal by the rough tops of the ice lenses and refrozen melt surface cause the bright returns from this region. This interpretation is in close agreement with the results of field measurements (*5*) taken in the percolation zone.

Below this region is a narrow zone of intermediate brightness: the wet snow zone. Here the snow has reached the melting point as a result of latent heat released by extensive refreezing of meltwater. The elevated temperature enhances compaction, which causes the firn to be denser than in the percolation zone. Benson found that the upper boundary of this zone occurred over a distance of a few kilometers and could be identified from a transition in the hardness of the snowpack, as measured by a penetrometer. Ice lenses are still present in this zone, but are probably less effective backscatterers because of the reduced penetration of the radar into the higher density firn.

The lowest zone on the ice sheet is the bare ice zone, which is a combination of glacier ice produced by compaction of snow at higher elevations and superimposed ice that forms by freezing of meltwater at the base of the firn. In winter images (Fig. 1) this region exhibits relatively low backscatter compared to that of the firn of the wet snow zone, which is frozen throughout at this time. The difference in backscatter presumably is a result of the smooth surface of the ice–new snow interface in the bare ice zone, and a rougher surface and greater volume scattering in the firn of the wet snow zone. The backscatter pattern in this region is inverted during the summer, when the water-soaked firn of the wet snow zone appears darker than the bare ice zone.

Some bright regions are caused by extreme roughness associated with crevassing. For example, in the lower right of Fig. 1, the bright areas on the ice are the crevassed margins and drainage area of Jakobshavns Isbræ, an extensively studied (*6*, *7*) major outlet glacier in western Greenland. The margins of this glacier are heavily crevassed because of the velocity contrast of several kilometers per year between flow in the main channel and the surrounding ice.

The winter images used to produce Fig. 1 are free from the complicating presence of meltwater, revealing only the effects of melt-related diagenesis on the snowpack. Imagery acquired during the summer shows the effects of melt at lower elevations, where the presence of water substantially reduces the backscatter and makes the determination of zone boundaries more difficult.

Mosaic of Greenland

Comparison of the winter images in Fig. 1 with the mosaic of ERS-1 SAR imagery of Greenland acquired during one 35-day cycle that began on 1 August 1992 (Fig. 2) (8) reveals little difference at higher elevations but shows the effect of melt at lower elevations. The images in the August mosaic were acquired at the end of the melt season; there was still water-saturated firn in some parts of the wet snow zone, but most melting in the percolation zone had ceased.

The dry snow zone and percolation zone are clearly apparent at the resolution of Fig. 2. The wet snow zone, which is somewhat difficult to see at this scale, appears as a narrow band slightly darker than and at the outer (lower elevation) edge of the percolation zone, and the bare ice zone is the darker region outside of this. The bare ice zone, at this resolution, is much more homogeneous in appearance than the ice-free bedrock of the coastal areas.

The full-resolution (30-m) data set provided by the imagery used to produce this mosaic makes it is possible to locate the boundaries of several of these zones to within a few kilometers. The full-resolution data show that the transitions from the bare ice zone to the wet snow zone and from the wet snow zone to the percolation zone are distinct, although locally complex because of interfingering. This data set, which is an accurate map of the ice sheet, provides a baseline against which future variations in surface characteristics can be detected.

Large Flow Feature

The August mosaic reveals a large flow feature in northeast Greenland (Figs. 2 and 3). Visible band Advanced Very High Resolution Radiometer (AVHRR) imagery (not shown) indicates that the local relief of the feature is much larger than that of the areas to either side. This enhanced surface topography, as well as the distinct edges of the feature, must be dynamically generated by enhanced ice flow (9). SAR imagery of the feature shows backscatter variation with a spatial scale that is similar to the variation in the AVHRR imagery; however, the backscatter variations are related, at least in part, to snowpack properties rather than directly to surface slope as they are in visible imagery.

The faint streaky character of the margins in full-resolution SAR imagery suggests that the margins are sites of shear strain, which elongates features within the region where the velocity gradient is high. Near the coast, the margins change character and are distinctly crevassed where the flow divides around a ridge. The effects of this crevassing are visible for as much as 100 km

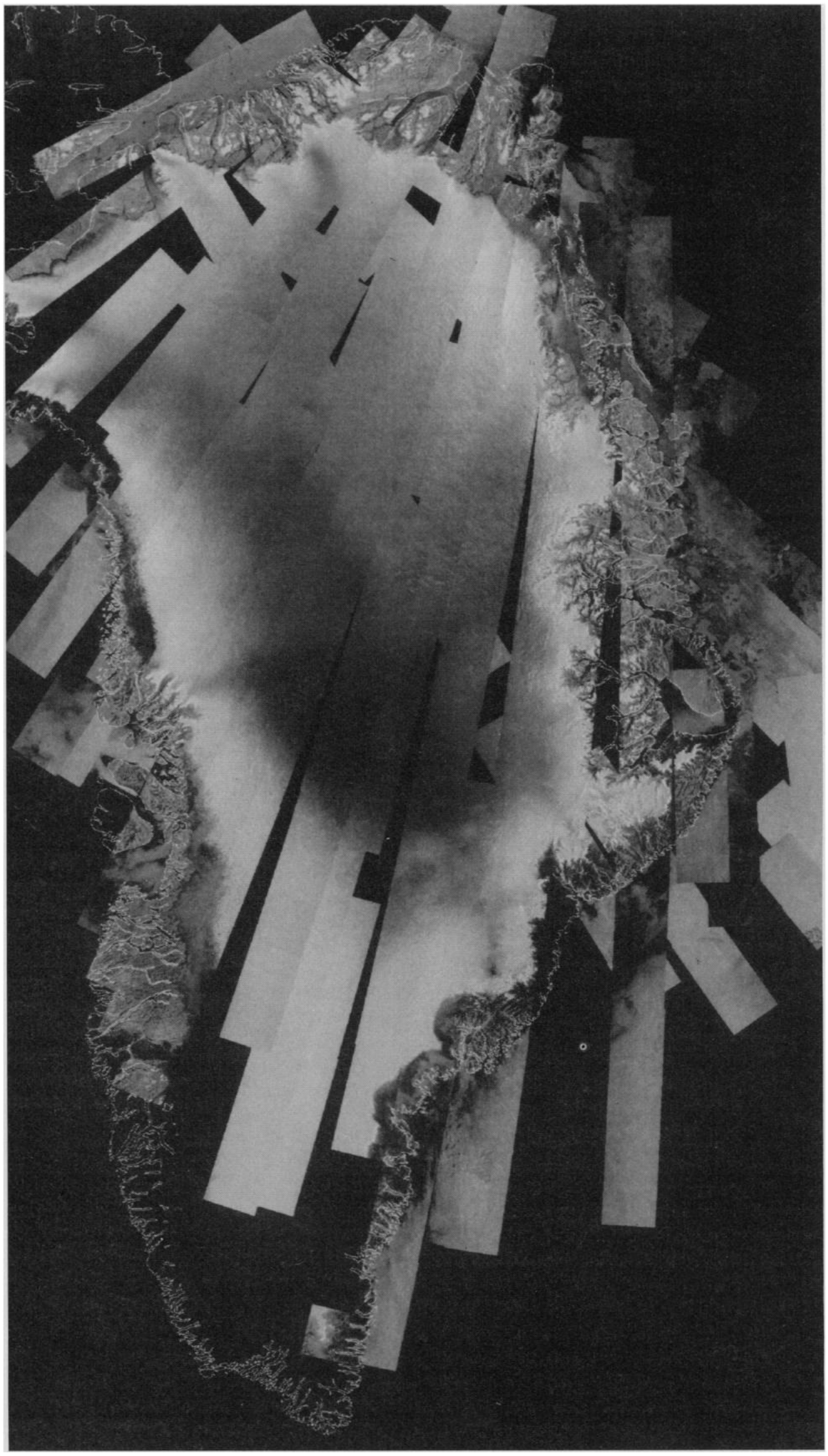

Fig. 2. Mosaic of August 1992 ERS-1 SAR imagery of the Greenland Ice Sheet. The mosaic is in the SSM/I polar stereographic projection. A coastline has been superimposed in white. Details of the mosaic are discussed in the text.

downstream as dark bands in the SAR imagery of this area (Fig. 3B), which is in the percolation zone (*10*).

The feature clearly originates well into the ice sheet, some 550 km from the coast, and flows north-northeastward. From an initial width of ~20 km, the feature widens symmetrically downslope, becoming ~70 km wide 400 km from the coast. This width is maintained for 150 to 200 km, until it becomes more difficult to identify the margins because of a rougher regional surface produced by the higher surface slope and reduced ice thickness near the edge of the ice sheet.

The feature is located along the axis of a broad topographic basin that can be seen in a recent digital elevation model of the ice sheet (*4*). This location suggests that the feature plays an important role in the ice dynamics of this region and may be responsible for the morphology of the basin. There is little information available about flow rates for the feature, except for a velocity of 500 m/year near the grounding line for Zachariæ Isstrøm (*11*), which is one of the branches that carries ice from the feature to the coast.

The topographic expression and large size of this feature are distinct; it is larger than Jakobshavns Isbræ and apparently has a larger drainage basin (*12*). In the mosaic of Fig. 2 the topographic expression related to Jakobshavns Isbræ only reaches a few hundred kilometers inland from the coast. It may be that Jakobshavns Isbræ has an equivalent or greater ice discharge, but the mechanics of the flow of the two features seem to be fundamentally different.

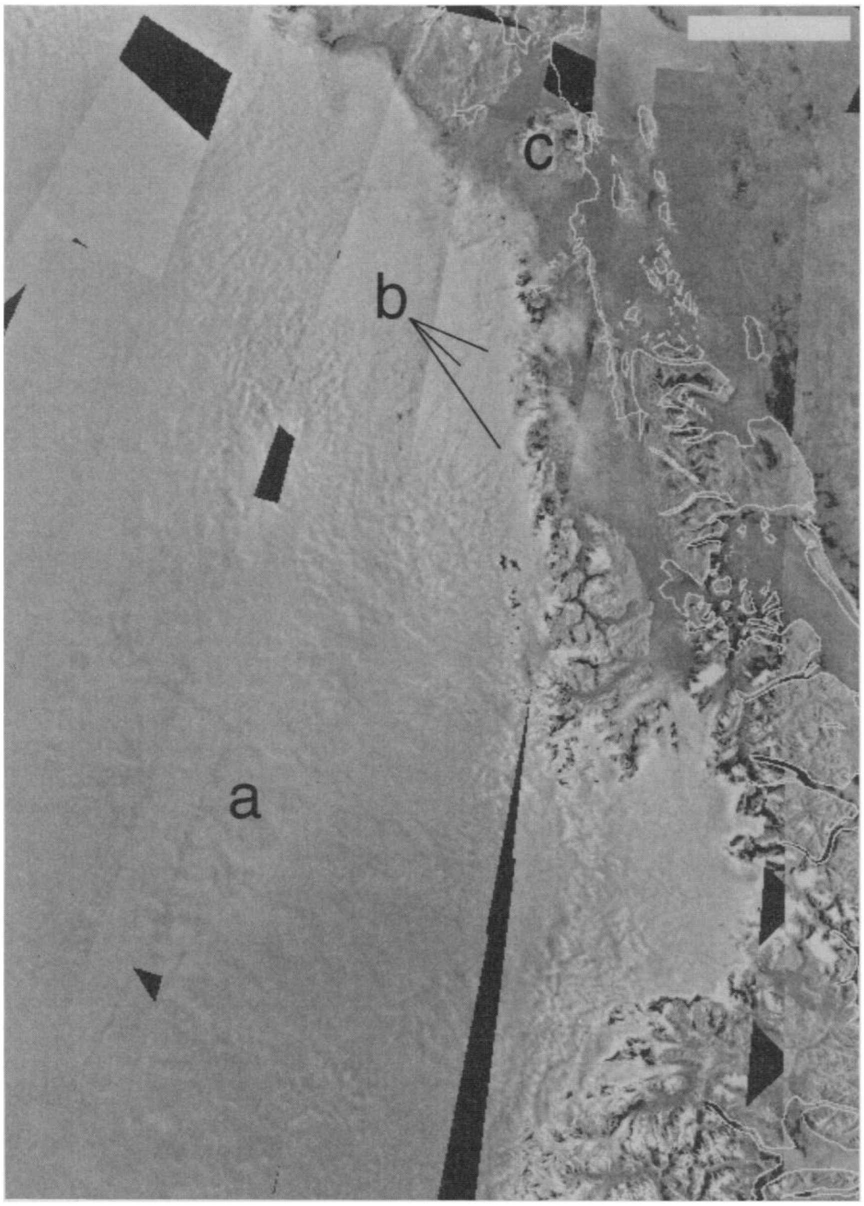

Fig. 3. Enlargement of Fig. 2, showing a large flow feature in northeast Greenland. Scale bar 100 km. a, flow feature; b, crevasse trains related to flow around a topographic high; c, Lambert Land.

The feature is morphologically closer to the ice streams of the Siple Coast of Antarctica than to Jakobshavns Isbræ. Comparison of Fig. 3 with an AVHRR image of the Siple Coast ice streams (*13*) shows that the features are of similar scale, with similar widths and distinct margins along some part of their lengths. There are several differences: the Siple Coast ice streams have heavily crevassed chaotic zones along much of their margins; they also begin in broad drainage regions, or catchments, where rapid flow starts at a number of points. This pattern is in contrast to the narrow, well-defined upper segment of the feature in northeast Greenland, which initiates near the ice divide. The subtle expression of the margins of the feature in its upper reaches suggests that the contrast in ice-flow velocity between the feature and its surroundings is less than the contrast seen over much of the length of the Siple Coast ice streams, which is several hundred meters per year.

Sequential SAR Imagery

The ability of SAR to image the surface without interference from cloud cover and darkness makes it an ideal tool for the systematic study of ice-sheet properties that vary with time. We used this capability to monitor the changes in the snow zones during the transition from the melt season to winter during 1992. The changes observed are a result of water draining out of, or freezing in, lakes, the snow pack, and the surface ice in the bare ice zone. In addition, there are changes in the images that are produced by ice motion.

Regions in early August images in the water-soaked wet snow zone appear dark because of the free water contained in the snowpack. These same regions are brighter than the ice in the surrounding area during the winter when there is no free water. This inversion of the backscatter pattern occurred between 17 August and 26 October 1992. The intermediate image in this sequence (21 September) shows a reduced contrast between the two areas. The August mosaic (Fig. 2) shows the effect of time variation of the backscatter signature in the wet snow zone between adjacent swaths. This variation produces visible edges to the swaths because areas that were melted at the time of a first pass were frozen and brighter at the time of an overlapping pass. It is not yet known to what depth the snowpack must refreeze in order to produce increased backscatter, but this depth and the rate of freezing must depend on local climatic variables.

Winter images show less month-to-month variation, and interpretation of the backscatter pattern is simplified by the

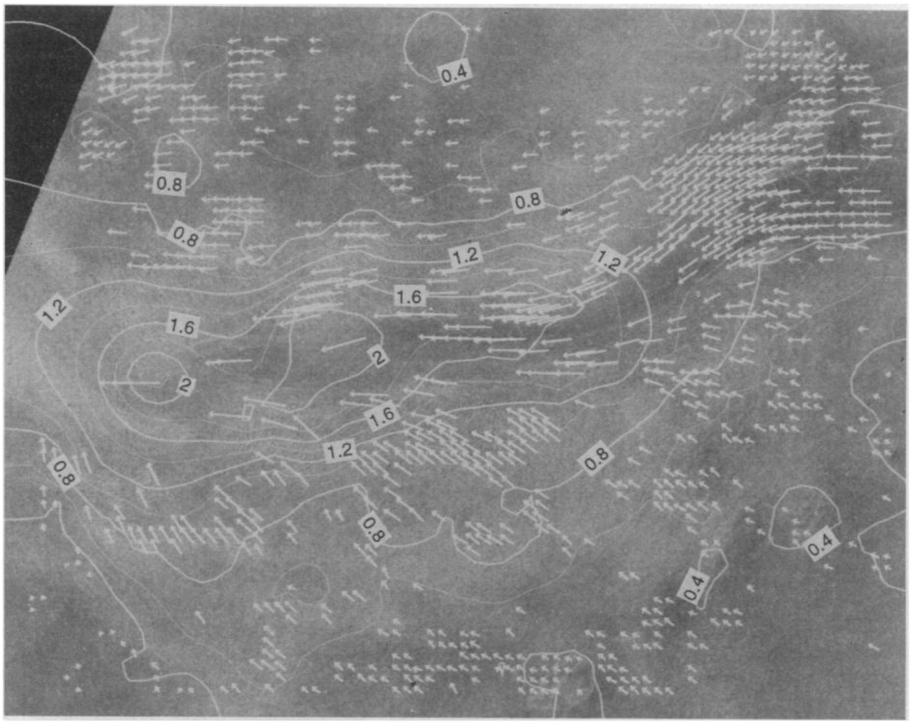

Fig. 4. Surface ice flow field of Jakobshavns Isbræ derived by computer determined displacements of features in two images acquired 105 days apart. Vectors indicate flow direction and speed. Contours show speed in kilometers per year, with a contour interval of 0.2 km/yr. The main channel is the sinuous dark area, bounded by brighter crevassed regions, which flows from the upper right to the middle left. North is toward the top of the image. The scene size is 16 km by 12 km.

lack of meltwater. The extent of the snow zones in winter images is the same as the extent at the end of the melt season, as new snow has little effect on the backscatter signature.

Tracking ice motion. It is possible to follow the displacements of features such as crevasses and lake shorelines in sequential SAR images. Computer matching of features allows a detailed surface velocity field to be determined (*14*). Fields of surface velocity produced in this way are useful for understanding the dynamics of rapid discharge from large ice sheets. Results for the middle reach of Jakobshavns Isbræ (Fig. 4) show that the ice flow in this area is extremely rapid; velocities are as high as 2 km/year. The rapid flow makes it possible to map the displacement field with the use of a short time interval between SAR frames (105 days in this case). The accuracy of the velocities is about ±80 m/year based on a one-pixel misregistration between the two images; this error is proportional to the inverse of the time interval.

The main stream of ice shown in Fig. 4 contributes a large part of the flux to the calving face of Jakobshavns Isbræ (*6*). Flow immediately to the north of the stream (upper part of Fig. 4) is generally parallel to the flow direction in the stream, whereas flow to the south is strongly convergent. This velocity field, when combined with information about surface slope and ice thickness, will allow detailed modeling of conditions governing the ice discharge in this area.

It is clear that SAR provides useful glaciological information, but this information is complementary to what is available from other satellite-based systems. SAR provides much higher resolution than passive microwave sensors such as The Special Sensor Microwave/Imager, but with less frequent coverage and without a sensitivity to temperature. A combination of the data from both active and passive microwave sensors provides a better view of the properties of the snowpack. Although high-resolution visible sensors provide higher quality data for mapping velocity fields (less distortion from topography, absence of the speckle inherent in imaging radar), SAR acquisition is possible through cloud cover and in darkness, making it a reliable source of images for these studies.

REFERENCES AND NOTES

1. Mass balance is the mass rate of change of the ice per unit area. When considered on a local scale, it includes snowfall, ablation, and the gradient of ice velocity; for an entire ice sheet, it is a measure of overall change in mass.
2. C. Benson, *Cold Reg. Res. Engin. Lab. Rep. 70* (1962); C. Benson, *Folia Geograph. Danica* **9**, 13 (1961).
3. A 1 K shift in temperature with a typical atmospheric lapse rate for Greenland of 1 K/100 m elevation and a surface slope of 0.01, typical for the lower elevations of the Greenland Ice Sheet, would produce a 10-km lateral shift of the isotherm at the ice surface.
4. The data were acquired 2 October 1991 and 3 March 1992 by the ERS-1 satellite, terrain-corrected, averaged to 1-km pixels, and draped over a digital elevation model of the region. Terrain correction is necessary because SAR is a side-looking instrument; this means that any topographic relief in the field of view introduces a geometric distortion in uncorrected imagery. The digital elevation model that was used for both the terrain correction and topography is a composite of Geosat, preliminary ERS-1 airborne radar altimetry, and digitized topographic maps produced by S. Ekholm at Kort-og Matrikelstyrelsen, Denmark.
5. K. Jezek and P. Gogineni, in preparation; E. J. Rignot, S. J. Ostro, J. J. van Zyl, K. C. Jezek, *Science* **261**, 1710 (1993).
6. K. Echelmeyer, T. S. Clarke, W. D. Harrison, *J. Glaciol.* **37**, 368 (1991).
7. A. Iken, K. Echelmeyer, W. Harrison, M. Funk, *ibid.* **39**, 15 (1993).
8. The mosaic of Fig. 2 was produced by mapping data into a polar stereographic projection based on the SSM/I grid. This projection has a standard latitude of 70°. The original imagery was averaged down to a pixel size of 1 km and corrected for pattern effects and topographic distortion before being mosaicked.
9. I. M. Whillans and S. J. Johnson, *J. Glaciol.* **29**, 78 (1993).
10. Crevassed areas in the percolation zone may appear dark because they interrupt the spatial coverage of the ice lenses, which provide a bright regional backscatter signature. As was previously mentioned, heavily crevassed areas in the wet snow and bare ice zones, such as the margins of Jakobshavns Isbræ, are brighter than their surroundings.
11. A. Higgins, *Rapport No. 140* (Grønlands Geologiske Undersøgelse, 1988), p. 102.
12. R. A. Bindschadler [*J. Geophys. Res.* **89**, 2066 (1984)] estimated that the size of the drainage basin for Jakobshavn was between 63,000 and 99,000 km^2, compared to approximately 180,000 km^2 for the flow feature in northeast Greenland.
13. R. A. Bindschadler and P. Vornberger, *Eos* **17**, 23 (1990).
14. T. Scambos, M. J. Dutkiewitz, J. C. Wilson, R. A. Bindschadler, *Rem. Sens. Environ.* **42**, 177 (1993).
15. We thank K. Arrigo and P. Vornberger for reviewing the manuscript, and S. Ekholm for making his elevation model available for terrain correction. The SAR data used in this article is copyrighted by ESA and used with permission. This work was conducted while M. Fahnestock was a National Research Council Research Associate. The work was supported by NASA's office of Mission to Planet Earth.